Generation of Accurate DEMs Using DInSAR Methodology (TopoDInSAR)

Oscar Mora, *Member, IEEE*, Roman Arbiol, Vicenç Palà, Albert Adell, and Marga Torre

***Abstract*—This letter presents a new methodology for the generation of digital elevation models (DEMs) by means of differential interferometry (DInSAR) algorithms with no need for classical phase unwrapping. During the last years, several advanced DInSAR proposals have been published, most of them based on a linear deformation adjustment together with topographic error estimation. In those cases, the input data are composed of a set of differential interferograms with different temporal gaps. Consequently, interferograms are affected by severe problems of temporal decorrelation, and the estimation of the topography can only be performed over coherent pixels, which are sparsely spread over the image. The proposal presented in this letter consists in the usage of a set of highly coherent topographic interferograms as input data for an advanced DInSAR algorithm. Then, using classical linear model adjustment, a detailed DEM of the observed area is estimated. This methodology is presented jointly with results obtained by processing real data acquired by European Remote Sensing satellites 1 and 2.**

***Index Terms*—Differential interferometry (DInSAR), digital elevation model (DEM), SAR interferometry (InSAR), synthetic aperture radar (SAR), topography.**

I. Introduction

THE APPLICATION of advanced differential interferometry (DInSAR) techniques has been restricted to the measurements of terrain displacements [1]–[6]. These techniques work with a stack of differential interferograms in order to minimize undesired phase components, such as atmospheric artifacts [7], [8], and obtain a precise measurement of the terrain displacement and topographic error. In most cases, a linear model is applied to calculate the mean displacement velocity and the topographic error of the digital elevation model (DEM) that was used to remove topography from the original interferograms.

The redundant data allow us to obtain precise measurements of the topographic differences, but only over those points with a high phase quality [1]–[6]. This limitation results in a sparse distribution of pixels over the whole area, where the topography can be estimated. Nevertheless, it would be desirable to obtain a topographic measurement over most points of the image. This letter presents the usage of the advanced DInSAR algorithm (DISICC) [1], [5], which is developed at the Institut Cartogràfic de Catalunya (ICC) to obtain precise DEMs through a stack of highly coherent topographic interferograms, i.e., 35-day or Tandem, instead of the group of differential interferograms that are used in classical DInSAR studies. The advantage of the presented topographic DInSAR (TopoDInSAR) methodology is that no external DEM is necessary, and the reconstructed topography covers nearly all the pixels in the scene due to the short temporal gaps between interferograms. The fact that a phase unwrapping is substituted by a weighted integration of the estimated heights is another great advantage of the proposed approach.

Manuscript received October 10, 2005; revised May 8, 2006.

O. Mora, R. Arbiol, and V. Palà are with the Remote Sensing Department, Institut Cartogràfic de Catalunya, 08038 Barcelona, Spain (e-mail: omora@icc.es).

A. Adell and M. Torre are with the Software Development Department, Institut Cartogràfic de Catalunya, 08038 Barcelona, Spain.

Color versions of Figs. 1, 3, and 4 are available at http://ieeexplore.ieee.org.

Digital Object Identifier 10.1109/LGRS.2006.879563

II. Methodology

The methodology is based on the usage of the DISICC, which that estimates the mean velocity and topographic residues from a stack of interferometric phases [1], [5]. When generating an interferogram by combining two synthetic aperture radar (SAR) images, its phase variation between neighboring pixels can be expressed as

$$\delta\phi_{\text{int}} = \delta\phi_{\text{flat}} + \delta\phi_{\text{topo}} + \delta\phi_{\text{mov}} + \delta\phi_{\text{atm}} + \delta\phi_{\text{noise}} \quad (1)$$

where $\delta\phi_{\text{flat}}$ Earth is the flat-earth component related with a range distance, $\delta\phi_{\text{topo}}$ is the topographic phase, $\delta\phi_{\text{mov}}$ is the component due to the displacement of the terrain in range direction [line of sight (LOS)] between both SAR acquisitions, $\delta\phi_{\text{atm}}$ is the phase related with atmospheric artifacts, and $\delta\phi_{\text{noise}}$ comprises degradation factors related with temporal and spatial decorrelation and thermal noise. When removing the flat Earth, we obtain the following TopoDInSAR phase:

$$\delta\phi_{\text{TopoDInSAR}} = \delta\phi_{\text{mov}} + \delta\phi_{\text{topo}} + \delta\phi_{\text{atm}} + \delta\phi_{\text{noise}}. \quad (2)$$

If a set of TopoDInSAR interferograms of the same area is used, a model, which considers a linear velocity deformation and topography, can be fitted to the stack of interferograms with different spatial and temporal baselines [1]. Note that no reference DEM is used for the generation of phases calculated in (2), as mentioned in Section I.

The TopoDInSAR model cannot be applied to all the pixels within the area under study, since only a part of them have the sufficient phase quality due to decorrelation. If short temporal baseline interferograms are used, the percentage of useful pixels will be very high and enough for topographic purposes.

In most cases, the deformation term will be very low in comparison with the topographic one. Nevertheless, if terrain movement is very strong, interferograms with short temporal baselines will present deformation fringes, and the movement term must be computed for precise estimation of topography.

First, pixel selection, which is based on the phase quality, has to be performed before computing the topography and deformation velocity. This selection can be done with a method based on a spatial coherence [1]. The spatial coherence is used to obtain the maximum-likelihood estimator of the coherence magnitude and provide an estimation of the accuracy of the pixel's phase for each interferogram that is not dependent on the number of images available. In DISICC, pixels in multilooked images are selected from their coherence stability using the mean coherence image generated from the whole stack of coherence maps.

After that, in order to obtain high-quality data free of unknown phase offsets [1], pixels are related by means of the Delaunay triangulation [9], [10]. This kind of triangulation relates all the neighboring pixels of irregularly gridded data generating nonoverlapped triangles. Another advantage of relating neighboring pixels is that the atmospheric component is minimized for every relationship due to their spatial proximity [1]. This assumption holds if during triangulation, the maximum distance allowed to connect two separate pixels is limited to approximately 1 km, which is a reasonable correlation distance of the atmosphere [7], [8]. Note that when using short temporal baseline interferograms, the distance between neighboring coherent pixels will be usually one pixel. As the topography and linear velocity are constants in the whole set of differential interferograms, it is possible to retrieve a good estimation of them, adjusting the following phase model to data [1]–[6]:

$$\begin{aligned}&\delta\phi_{\text{model}}(x_{\text{m}}, y_{\text{m}}, x_{\text{n}}, y_{\text{n}}, T_i)\\&= \frac{4\pi}{\lambda}\cdot T_i\cdot[v_{\text{model}}(x_{\text{m}}, y_{\text{m}}) - v_{\text{model}}(x_{\text{n}}, y_{\text{n}})] + \frac{4\pi}{\lambda}\\&\quad\cdot\frac{b(T_i)}{r(T_i)\cdot\sin(\theta_i)}\cdot[h_{\text{model}}(x_{\text{m}}, y_{\text{m}}) - h_{\text{model}}(x_{\text{n}}, y_{\text{n}})]\end{aligned}\tag{3}$$

where λ is the wavelength, T_i is the temporal gap for each interferogram, v_{model} is the linear velocity, b is the spatial baseline, r is the distance between the satellite and terrain, θ_i is the incidence angle, h_{model} is the topography, and $(x,\ y)$ the position of the pixel inside the interferogram. Then, the adjustment can be performed maximizing the following model coherence function [6]:

$$\begin{aligned}&\gamma_{\text{model}}(x_{\text{m}}, y_{\text{m}}, x_{\text{n}}, y_{\text{n}})\\&= \frac{1}{N}\cdot\left|\sum_{i=0}^{N}\exp\left[j\cdot\left(\delta\phi_{\text{TopoDInSAR}}\left(x_{\text{m}}, y_{\text{m}}, x_{\text{n}}, y_{\text{n}}, T_i\right)\right.\right.\right.\\&\qquad\left.\left.\left.-\ \delta\phi_{\text{model}}\left(x_{\text{m}}, y_{\text{m}}, x_{\text{n}}, y_{\text{n}}, T_i\right)\right)\right]\right|\end{aligned}\tag{4}$$

where N is the number of interferograms. This function is equal to one when the adjustment to data is perfect and zero in case of total decorrelation. Once this maximization process has been done for each relationship, the result is a set of topography and velocity increments [1].

After that, an integration process is necessary to obtain absolute height values for each pixel. A classical region growing approach can be used for this purpose [11]. The integration starts from different seed points, which is chosen from those presenting links with better model coherences, and calculates the absolute topography for each pixel using

$$\begin{aligned}h_{\text{estimated}}(x,y) = &\frac{1}{\sum_i \gamma_{\text{model}}(x,y,x_i,y_i)}\\&\cdot\sum_i\left[h_{\text{estimated}}(x_i,y_i)\right.\\&\qquad\left.+\ \Delta h_{\text{estimated}}(x,y,x_i,y_i)\right]\\&\cdot\gamma_{\text{model}}(x,y,x_i,y_i)\end{aligned}\tag{5}$$

where index i corresponds to those neighboring pixels connected to the one that is being integrated. Each contribution reaching a pixel is weighted with its associated model coherence to reduce the contribution of the less reliable connections. If strong terrain displacements are present in the area under study, the velocity term can be computed in a similar way.

As a conclusion, it is very important to have a homogeneous distribution of spatial baselines to correctly compute the topography. Moreover, if our goal is the generation of DEMs, the best results are obtained with a selection of short temporal baselines, which allow to generate interferograms with a lower temporal decorrelation, and thus select a larger number of coherent pixels. Despite the fact that velocity estimation will be less reliable, as short temporal baselines reduce their impact on phase, the estimation of topography will be more reliable.

TABLE I
LIST OF INTERFEROGRAMS

Interferogram	Master	Slave	Baseline (m)
1	27/12/1992	31/01/1993	75
2	31/10/1995	01/11/1995	100
3	28/05/1996	29/05/1996	108
4	14/12/1999	15/12/1999	187

III. RESULTS

This section presents the results obtained using a set of real data from the European Remote Sensing 1 and 2 (ERS-1/2) satellites. The area under study corresponds to the Bages zone, in Catalonia. Table I shows the list of the four topographic interferograms used in this study. As presented in Table I, the distribution of baselines is not homogeneous, since three of the four values are greater than 100 m. On the other hand, the number of interferograms is also low. Obviously, this fact depends on the availability of suitable images for generating interferograms with short temporal gaps. Fig. 1 presents the four interferograms for different baselines. Note the higher fringe frequency for the interferograms with lager baselines.

Fig. 2 shows the coherence image generated by averaging the stack of coherences from the interferograms listed in Table I. White pixels present the maximum coherence and quality, and black pixels are totally decorrelated. After applying a threshold of 0.25 in the selection processing, more than 99% of points have been selected, and the majority of pixels will be processed. Thus, a continuous DEM will be obtained.

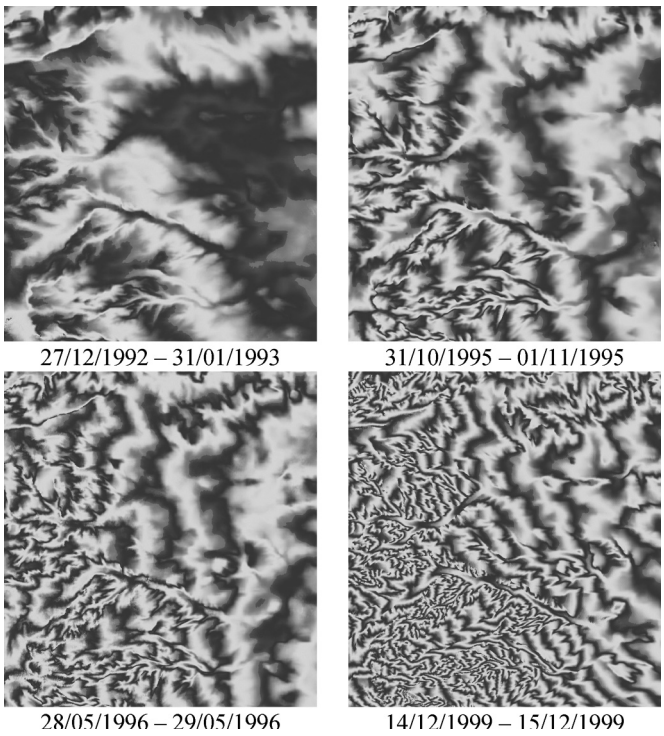

Fig. 1. Set of four interferograms used in this letter (see Table I).

Fig. 2. Coherence average image obtained using the interferograms presented in Table I.

Due to pixel density, selected points and Delaunay networks are not presented graphically. Fig. 3 shows the topographic model obtained after executing the DISICC software with the data presented in Table I. The DEM has been projected over the ED50 ellipsoid and expressed in UTM coordinates. The robustness of the algorithm is very high, since the percentage of selected pixels that are correctly integrated using (5) is 98%.

Once the DEM has been generated using the methodology described in the previous section, a comparison with other sources must be done to obtain an estimation of the height quality. In this case, the comparison has been performed with the homologous DEMs of the ICC and Shuttle Radar Topography Mission (SRTM) [12].

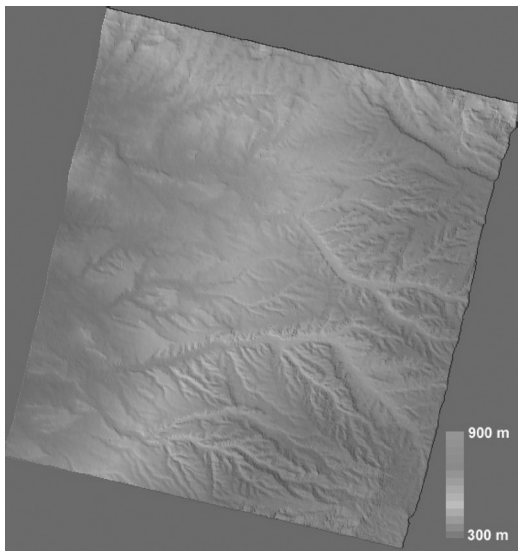

Fig. 3. Topographic model of Bages area obtained by means of TopoDInSAR methodology. The height ranges from 300 to 900 m. The DEM has been projected over the ED50 ellipsoid and expressed in UTM coordinates.

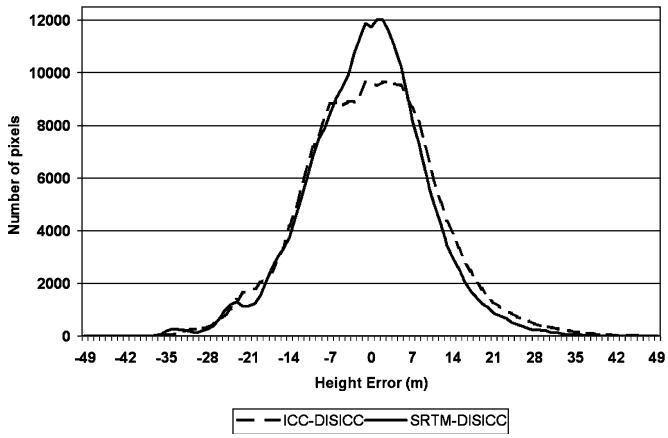

Fig. 4. Histograms of the two height difference images. Comparison between ICC DISICC and SRTM DISICC error maps.

TABLE II
STATISTICAL STUDY OF DEMs DIFFERENCES

Pair	Mean (m)	Standard Deviation (m)	Max. difference (m)
ICC-TopoDInSAR	0.42	11.06	57.02
SRTM-TopoDInSAR	-0.28	9.97	60.09
ICC-SRTM	0.52	3.75	35.13

The histograms of the two height difference maps regarding the TopoDInSAR map are presented in Fig. 4 for the comparisons with ICC and SRTM DEMs, respectively. Table II also summarizes the results of these comparisons showing the mean, standard deviation, and maximum value of the height differences. In all cases the mean difference is of some centimeters; therefore, it can be considered that there is no bias between the three DEMs.

On the other hand, the standard deviation is slightly different in the three cases. The SRTM DEM is more similar to the

TopoDInSAR one, presenting a standard deviation lower than 10 m, while the ICC map differs with a deviation greater than 11 m. This could be explained because of the similarities in the original data for the SRTM and TopoDInSAR cases, since both are generated using InSAR techniques and correspond to digital surface models. Note that the ICC topographic map is a digital terrain model that has been created using optical data. Table II also shows that the height differences between the ICC and SRTM maps are lower, because the number of images used to generate the SRTM's DEM is larger than the one used to generate the TopoDInSAR topography presented in this letter [13].

IV. Conclusion

In this letter, the idea of using new advanced DInSAR algorithms for estimating ground displacements has been extended to the generation of full topographic maps. Taking advantage of the qualities of the DISICC software implemented in the ICC, accurate DEMs can be obtained from a stack of classical topographic interferograms. The following are main advantages of this methodology.

1) Minimization of the atmospheric artifacts due to data redundancy and triangulation of neighboring point.
2) Classical phase unwrapping is not necessary, because the phase model [see (3)] is directly applied on the differential topographic wrapped phases between the adjacent pixels.

As commented in Section II, the best data configuration is composed by a uniform distribution of baselines not exceeding the limits for spatial decorrelation. Obviously, the larger the number of interferograms, the better the final quality of the DEM. Finally, an experiment with real data from ERS-1/2 satellites has been performed, confirming the suitability and possibilities of the TopoDInSAR methodology. Further developments must be done in order to test the methodology with a larger number of interferograms and combination of ERS and ENVISAT data.

Acknowledgment

The authors would like to thank the Interreg IIIB-MEDOCC program for the ERS-1/2 images provided in the RISCMASS project, which have been used for this study. The authors would also like to thank the reviewers for their very interesting proposals to improve this letter.

References

[1] O. Mora, J. J. Mallorquí, and A. Broquetas, "Linear and nonlinear terrain deformation maps from a reduced set of interferometric SAR images," *IEEE Trans. Geosci. Remote Sens.*, vol. 41, no. 10, pp. 2243–2253, Oct. 2003.

[2] R. Lanari, O. Mora, M. Manunta, J. J. Mallorquí, P. Berardino, and E. Sansosti, "A small-baseline DIFSAR approach for investigating deformations on full-resolution SAR interferograms," *IEEE Trans. Geosci. Remote Sens.*, vol. 42, no. 7, pp. 1377–1386, Jul. 2004.

[3] P. Berardino, G. Fornaro, R. Lanari, and E. Sansosti, "A new algorithm for surface deformation monitoring based on small baseline differential SAR interferograms," *IEEE Trans. Geosci. Remote Sens.*, vol. 40, no. 11, pp. 2375–2383, Nov. 2002.

[4] A. Ferretti, C. Prati, and F. Rocca, "Permanent scatterers in SAR interferometry," *IEEE Trans. Geosci. Remote Sens.*, vol. 39, no. 1, pp. 8–30, Jan. 2001.

[5] O. Mora, V. Palà, R. Arbiol, A. Adell, and M. Torre, "Medidas de deformación del terreno a vista de satélite," in *Congr., Nacional de Teledetección*. Tenerife, Spain, Sep. 21–23, 2005.

[6] A. Ferretti, C. Prati, and F. Rocca, "Nonlinear subsidence rate estimation using permanent scatterers in differential SAR interferometry," *IEEE Trans. Geosci. Remote Sens.*, vol. 38, no. 5, pp. 2202–2212, Sep. 2000.

[7] R. Hanssen, *Atmospheric Heterogeneities in ERS Tandem SAR Interferometry*. Delft, The Netherlands: Delft Univ. Press, 1998.

[8] ——, *Radar Interferometry*. Norwell, MA: Kluwer, 2001.

[9] B. Delaunay, "Sur la sphere vide," in *Bull. Acad. Sci. USSR (VII), Classe Sci. Mat. Nat.*, 1934, pp. 793–800.

[10] M. Costantini and P. A. Rosen, "A generalized phase unwrapping approach for sparse data," in *Proc. IGARSS*, Hamburg, Germany, Jun./Jul. 1999, vol. 1, pp. 267–269.

[11] W. Xu and I. Cumming, "A region-growing algorithm for InSAR phase unwrapping," *IEEE Trans. Geosci. Remote Sens.*, vol. 37, no. 1, pp. 124–134, Jan. 1999.

[12] *The USGS Shuttle Radar Topography Mission: Information About the Final Data Coverage Maps*. [Online]. Available: http://srtm.usgs.gov/data/coveragemaps.html

[13] C. G. Brown, K. Sarabandi, and L. E. Pierce, "Validation of the Shuttle Radar Topography Mission height data," *IEEE Trans. Geosci. Remote Sens.*, vol. 43, no. 8, pp. 1707–1715, Aug. 2005.